J|A|C|S ARTICLES

Published on Web 04/01/2009

Cleavage of Carbon Dioxide by an Iridium-Supported Fischer Carbene. A DFT Investigation

Nigel J. Brookes,[†] Alireza Ariafard,[†,§] Robert Stranger,[‡] and Brian F. Yates*[,†]

School of Chemistry, University of Tasmania, Private Bag 75, Hobart, Tasmania 7001, Australia, Department of Chemistry, The Australian National University, Canberra ACT 0200, Australia, and Department of Chemistry, Faculty of Science, Central Tehran Branch, Islamic Azad University, Shahrak Gharb, Tehran, Iran

Received November 28, 2008; E-mail: brian.yates@utas.edu.au

Abstract: The reaction of CO_2, OCS, and PhNCO with an iridium-supported Fischer alkoxycarbene has been investigated with density functional theory. We have confirmed the mechanism for the important CO_2 reaction and successfully rationalized the selective cleavage of the CS and CN bonds in OCS and PhNCO. Armed with this information we have used our model to predict that the same iridium system will preferentially cleave the CS bond in methyl thiocyanate (MeNCS) rather than the CN bond. The formation of the iridium-supported carbene itself has also been investigated and a fascinating autocatalytic mechanism has been discovered which nicely fits the observed experimental behavior.

Introduction

The scission of small multiply bonded molecules has attracted much interest over the past 15 years with the significant discovery of N_2 cleavage using $Mo[N(R)Ar]_3$ ($R = C(CD_3)_2CH_3$, $Ar = 3,5\text{-}C_6H_3Me_2$)[1] and $Mo[(HIPTNCH_2CH_2)_3N]_3$ ($HIPT = 3,5\text{-}(2,4,6\text{-}{}^iPr_3C_6H_2)_2C_6H_3$))[2] exemplifying this area. Recently attention has shifted to the reactivity of 'environmentally important' carbon dioxide.[3−11] Given that CO_2 is widely blamed for global warming,[12] its breakdown or sequestration could have significant benefits for future generations.

A very recent study in the area of CO_2 breakdown has been performed by Whited and Grubbs[13] at Caltech where a previously synthesized[14] iridium-supported Fischer alkoxycarbene has been found to transfer the oxygen from CO_2, forming *t*-butyl formate and an iridium carbonyl complex (Scheme 1).

Scheme 1

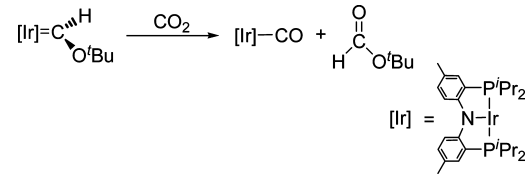

Scheme 2

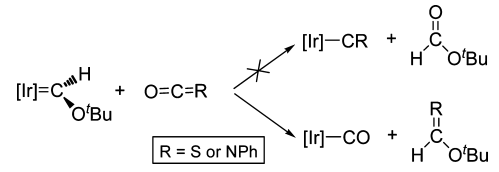

Interestingly the same reaction, but with carbonyl sulfide rather than CO_2, cleaves the CS bond, not CO (Scheme 2). With phenyl isocyanate, meanwhile, the CN is cleaved, not CO. The scission of CO, CS, and CN in CO_2, OCS, and PhNCO, respectively, has clear implications in transition metal catalysis and hence an exact picture of the reaction mechanism should be obtained.

Herein we describe the mechanism for oxygen-atom transfer from carbon dioxide to a Fischer carbene at (PNP)Ir (Scheme 1) using density functional theory. Cleavage of the CS and CN bonds in preference to CO in the reactions involving OCS and PhNCO has also been examined with DFT and the selectivity of the Fischer alkoxycarbene is explained.

Given the potential for catalytic activity of the (PNP)Ir=CO^{t}Bu moiety (although major barriers exist) it is pertinent to investigate in detail its formation (Scheme 3). For this reason in the first part of this paper we detail how the potential energy surface outlining the formation of

[†] University of Tasmania.
[‡] The Australian National University.
[§] Islamic Azad University.

(1) Laplaza, C. E.; Cummins, C. C. *Science* **1995**, *268*, 861–863.
(2) Schrock, R. R. *Chem. Commun.* **2003**, 2389–2391.
(3) Zhao, H.; Lin, Z.; Marder, T. B. *J. Am. Chem. Soc.* **2006**, *128*, 15637–15643.
(4) Sadique, A. R.; Brennessel, W. W.; Holland, P. L. *Inorg. Chem.* **2008**, *47*, 784–786.
(5) Arakawa, H.; et al. *Chem. Rev.* **2001**, *101*, 953–996.
(6) Darensbourg, D. J. *Chem. Rev.* **2007**, *107*, 2388–2410.
(7) Aresta, M.; Dibenedetto, A. *Dalton Trans.* **2007**, 2975–2992.
(8) Graham, D. C.; Mitchell, C.; Bruce, M. I.; Metha, G. F.; Bowie, J. H.; Buntine, M. A. *Organometallics* **2007**, *26*, 6784–6792.
(9) Graham, D. C.; Bruce, M. I.; Metha, G. F.; Bowie, J. H.; Buntine, M. A. *J. Organomet. Chem.* **2008**, *693*, 2703–2710.
(10) Fullmer, B. C.; Fan, H.; Pink, M.; Caulton, K. G. *Inorg. Chem.* **2008**, *47*, 1865–1867.
(11) Laitar, D. S.; Muller, P.; Sadighi, J. P. *J. Am. Chem. Soc.* **2005**, *127*, 17196–17197.
(12) Gore, A. *An Inconvenient Truth: The Planetary Emergency of Global Warming and What We Can Do About It*; Rodale Books: New York, 2006.
(13) Whited, M. T.; Grubbs, R. H. *J. Am. Chem. Soc.* **2008**, *130*, 5874–5875.
(14) Romero, P. E.; Whited, M. T.; Grubbs, R. H. *Organometallics* **2008**, *27*, 3422–3429.

10.1021/ja809320x CCC: $40.75

Scheme 3

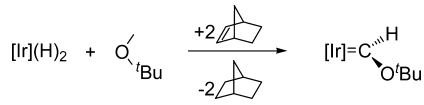

(PNP)Ir=CO^{t}Bu has been resolved, whereby a startling thermochemically driven mechanism has been discovered.

Computational Details

In order to adequately analyze the reaction profile of large transition metal complexes, a size-reduced model was employed throughout this study that mimics both atomic electronic behavior and molecular structure. The model has replaced the isopropyl and *tert*-butyl groups with methyl groups and replaced the aromatic rings with ethylene bridges. A diagram of the reduced model is provided in the Supporting Information, and the PNP iridium framework, as shown in Scheme 1, will be abbreviated by [Ir].

All geometry optimizations were performed using the hybrid density functional B3LYP[15−18] in combination with a general basis set (termed GBS1) employing LANL2DZ[19,20] on iridium and 6-31G(d)[21] on other atoms. All final geometries were optimized with unrestricted wave functions, and reoptimisation was carried out in those cases where wave function instabilities were observed. Five d-functions were used in the basis set throughout these calculations. Full conformer searching was carried out on all structures, and frequency calculations were performed with structures characterized as minima or transition states based on the observed number of imaginary frequencies. All transition structures contained exactly one imaginary frequency and were linked to reactant, products, or intermediates using intrinsic reaction coordinate (IRC) calculations.[22] Single point energy calculations on both model and real optimized geometries were performed with B3LYP using a larger basis set (termed GBS2) on iridium expanded to triple-ζ with the inclusion of diffuse (s,p,d) and polarization (f) functions, combined with 6-311+G(2d,p) on other atoms. Full details of the iridium basis set are provided in the Supporting Information. Comparison single point energies using BMK[23] and TPSS[24,25] functionals have also been carried out and are available in the Supporting Information. These functionals do not alter the overall conclusions from the B3LYP potential energy surface. Gibbs free energy and zero-point vibrational energy corrections taken from the B3LYP/GBS1 level of theory have been included on all B3LYP/GBS2 single point energy calculations, and all potential energy surfaces in this paper are reported at this final ΔG_{298} level of theory. Uncorrected electronic energies using the larger GBS2 basis set have been included in all diagrams in parentheses. Due to the expected low charge separation experienced throughout the reactions, solvent effects are not expected to play a major part in the reaction energetics. However, solvent corrections using IEFPCM[26] are available in the Supporting Information. They do not change the overall conclusions, but they do show a small lowering of the barrier for CO_2 cleavage. All Mulliken and NBO electron densities quoted in the text were calculated using the smaller GBS1 basis set. Details of the GBS2 basis set can be found in the Supporting Information. All calculations were carried out with the Gaussian03 set of programs.[27]

Results and Discussion

Validation of the B3LYP functional for transition metal complexes has been performed in the past by our group[28,29] and others,[30−33] but to add justification to this analysis, the optimized geometries for both [Ir]=C(H)O^{t}Bu and [Ir]−CO using the reduced model and full ligand system were compared to the published X-ray crystal data.[14] The predicted and experimental geometries are almost identical for both the full ligand and reduced model optimizations. These results and additional structural and energetic comparisons between the reduced model and full ligand system can be found in the Supporting Information. Energetic comparisons using BMK/GBS2 and TPSS/GBS2 applied to the geometries obtained using B3LYP/GBS1 have also been carried out. These results are available in the Supporting Information and closely match the mechanistic findings reported here using B3LYP/GBS2.

Formation of Iridium-Supported Fischer Carbene [Ir]=C(H)O^{t}Bu. Experimentally the formation of [Ir]=C(H)O^{t}Bu (**7**) occurs via the α,α-dehydrogenation of [Ir]H_2 (**1**) using norbornylene (Nor) in methyl *t*-butyl ether (MTBE). The MTBE adduct forms rapidly followed by double C−H activation and loss of H_2 over a 16 h period.[13,14] Interestingly 2 equiv of norbornylene are required to drive the reaction to completion, and it has been suggested that the second equivalent is required to simply remove the H_2 byproduct as it is formed. Our calculations indicate that the formation of **7**, in agreement with experimental evidence, does occur by an initial MTBE adduct, but that the overall mechanism is quite complex particularly in terms of the thermodynamic and kinetic driving force.

Figure 1 outlines the first part of the mechanism whereby the dihydride of **1** is removed by norbornylene leaving an active [Ir] (**2**) metal center. This can coordinate the ether via direct C−H activation to form [Ir]−H−CH_2O^{t}Bu (**4**). Figure 2 highlights the structure of **4** where a three-center, two-electron agostic interaction has increased the C−H bond length from 1.100 Å in MTBE to 1.157 Å. Oxidative addition then furnishes a stable [Ir](H)CH_2O^{t}Bu (**5**) intermediate, via an energetically 'flat' transition structure **4-TS** where the interacting C−H bond has been activated to 1.355 Å. As can be seen in Figure 1, the heat of reaction of **1** with norbornylene is endothermic by +48.7 kJ mol^{-1}, followed by a barrierless pathway directly to intermediate **5** via the agostic interaction seen in **4**. Clearly our calculation predicts a clean, rapid formation of intermediate **5**, a fact that is nicely matched by experimental findings.[14]

An alternate pathway does exist to formation of **5**, that being ether coordination via oxygen forming [Ir]−O(CH_3)^{t}Bu (**3**) followed by rearrangement through structure **3-TS** to the C−H

(15) Becke, A. D *Phys. Rev. A.* **1988**, *38*, 3098–3100.
(16) Becke, A. D. *J. Chem. Phys.* **1993**, *98*, 5648–5652.
(17) Lee, C; Yang, W.; Parr, R. G *Phys. Rev. B* **1988**, *37*, 785–789.
(18) Stephens, P. J.; Devlin, F. J.; Chabalowski, C. F.; Frisch, M. J. *J. Phys. Chem.* **1994**, *98*, 11623–11627.
(19) Hay, P. J.; Wadt, W. R. *J. Chem. Phys.* **1985**, *82*, 299.
(20) Wadt, W. R.; Hay, P. J. *J. Chem. Phys.* **1985**, *82*, 284–298.
(21) Hariharan, P. C.; Pople, J. A. *Theor. Chim. Acta* **1973**, *28*, 213–222.
(22) Gonzalez, C.; Schlegel, H. B. *J. Phys. Chem.* **1990**, *94*, 5523–5527.
(23) Boese, A. D.; Jan, M. L. M. *J. Chem. Phys.* **2004**, *121*, 3405–3416.
(24) Perdew, J. P.; Tao, J. M.; Staroverov, V. N.; Scuseria, G. E. *J. Chem. Phys.* **2004**, *120*, 6898–6911.
(25) Tao, J. M.; Perdew, J. P.; Staroverov, V. N.; Scuseria, G. E. *Phys. Rev. Lett.* **2003**, *91*, 146401.
(26) Tomasi, J.; Mennucci, B.; Cammi, R. *Chem. Rev.* **2005**, *105*, 2999–3094.
(27) Frisch, M. J.; et al. *Gaussian 03, Revision E.01*; Gaussian, Inc.: Wallingford, CT, 2004.
(28) Graham, D. C.; Beran, G. J. O.; Head-Gordon, M.; Christian, G.; Stranger, R.; Yates, B. F. *J. Phys. Chem. A* **2005**, *109*, 6762–6772.
(29) Brookes, N. J.; Graham, D. C.; Christian, G. J.; Stranger, R.; Yates, B. F. *J. Comput. Chem.* 2009, in press.
(30) Ziegler, T. *Chem. Rev.* **1991**, *91*, 651–667.
(31) Koga, N.; Morokuma, K. *Chem. Rev.* **1991**, *91*, 823–842.
(32) Morokuma, K.; Musaev, D. G.; Khoroshun, D. V.; Vreven, T.; Liu, Z. W.; Torrent, M.; Basch, H.; Yates, B. F.; Mori, S. *Abstr. Papers Am. Chem. Soc.* **2000**, *220*, U492–U492.
(33) Frenking, G.; Frohlich, N. *Chem. Rev.* **2000**, *100*, 717–774.

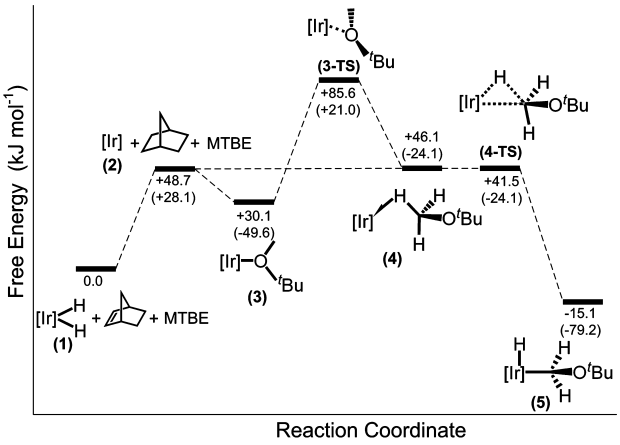

Figure 1. Potential energy surface for the formation of adduct [Ir](H)CH_2O^tBu (**5**). Values in normal script are Gibbs corrected and those in parentheses are uncorrected electronic energies. All values in kJ mol^{-1}.

activation seen in **4**. This pathway, as seen in Figure 1, is energetically unfavorable since the rearrangement involves a significant barrier of +85.6 kJ mol^{-1} at **3-TS**. It should also be noted in Figure 1 that **4**-**TS** appears slightly lower in energy than **4**. This is due to the entropy considerations present in the ΔG_{298} calculations, which are significant when the molecular numbers alter as seen throughout this reaction.

Figure 3 outlines the rearrangement and elimination reaction that **5** undergoes in forming the desired Fischer alkoxycarbene **7** (see the Supporting Information for detailed structures). Our calculations support initial α-hydrogen migration onto the metal center forming **6** in either the cis or trans configuration. The **6-trans** orientation is kinetically and thermodynamically more likely, while the **6-cis** has a significant barrier to formation of +57.7 kJ mol^{-1} (at **5-TS**) and leads to the carbene **7** plus H_2, through an even larger barrier of +76.2 kJ mol^{-1} as shown in Figure 3.

The close energetics of these species, **5** (−15.1 kJ mol^{-1}), **6-trans** (−21.9 kJ mol^{-1}), **6-cis** (+8.2 kJ mol^{-1}), and **7** + H_2 (+0.2 kJ mol^{-1}), is significant. Given no specific thermodynamic driving force, these calculations suggest, under equilibrium conditions, that **5** and **6-trans** would both be present, and given sufficient time, minor amounts of **6-cis** and **7** might also be detected. The experimental finding of carbene **7** as the major product of this reaction would certainly not be predicted by these calculations. There is clearly a missing component from this reaction sequence and it turns out that this comes from the interaction of the generated H_2 with **5**.

The low quantity of dihydrogen formed by the reductive elimination in Figure 3 is at first considered an annoying equilibrium reaction byproduct, since it doubles the quantity of norbornylene required to quantitatively complete the reaction. This is far from reality; in fact, it provides the reaction driving force mechanistically and thermodynamically. As outlined in Figure 4, the small quantity of dihydrogen produced by the equilibrium reaction in Figure 3 can react in a highly exothermic fashion with remaining intermediate **5.** This requires rearrangement of **5** such that the bound MTBE is perpendicular to the (PNP)Ir planar structure. This pseudorotation from **5** to **5b** and **5c** is energetically 'flat', and all conformers are likely to be present in equilibrium. Addition of dihydrogen can occur to either of the conformers with the lowest energy pathway being from **5b** or via **5c**. Both conformer interactions result in oxidative addition whereby the H_2 initially binds in the nonclassical form,[34] as seen in [Ir](η^2-H_2)(H)CH_2O^tBu (**8**), and rearranges via **8-TS** to the slightly preferred classical form[34] of [Ir]$(H)_3CH_2O^tBu$ (**9**). The trans influence of the now bound hydride weakens the [Ir]−C bond such that its length increases from 2.085 Å in **8** to 2.194 Å in **9**, thus allowing reductive elimination of MTBE through transition structure **9-TS,** where the Ir−C bond has further lengthened to 2.300 Å. This combination of oxidative addition and trans influenced reductive elimination results in a maximum barrier of just 37.0 kJ mol^{-1} (at **9-TS**) and furnishes the starting material **1** exothermically (−79.3 kJ mol^{-1}) along with unbound MTBE. This unusually flat pathway from **5** to **9-TS** is due to the stabilizing interaction between the three iridium bound hydrogens, and is critical for this reaction to proceed. This is certainly the preferred path as compared to the reverse equilibrium option in Figure 3, which has a barrier of +76.2 kJ mol^{-1} (Figure 3).

As with most reactions, an alternative pathway from **5** to **1** does exist. H_2 addition could occur from the ground-state structure of **5** as shown in Figure 5. This approach can coordinate the H_2 trans to the bound hydrogen as in structure **10** but unfortunately leads to a significant barrier at **10-TS** of +59.2 kJ mol^{-1}, which is some 22.2 kJ mol^{-1} higher that that shown above for **5b** and **5c**. The absence of a bound hydride trans to the MTBE leaving group is responsible for this increased energy barrier. The presence of excess MTBE solvent may also compete by combining explicitly with intermediate **5** to form analogues of **8** and **10** with H_2 replaced by MTBE, thus preventing H_2 access. Our calculations using dimethyl ether as a model for MTBE indicate that the solvent can indeed combine with intermediate **5**, but this is energetically less favorable by 53.4 (for the analogue of **8**) and 26.9 kJ mol^{-1} (for the analogue of **10**) than coordination of H_2 (see the Supporting Information). Part of the reason for this preference for H_2 rather than MTBE coordination is the steric effect of the bulky phosphine ligands.

The importance of the low-energy transition structures, the exothermicity provided by the H_2 reaction and the equilibrium interplay between species **5**, **6** (cis and trans), and **7** cannot be overemphasized. Without all three of these features present, the Fischer alkoxycarbene **7** would not be produced except in minute

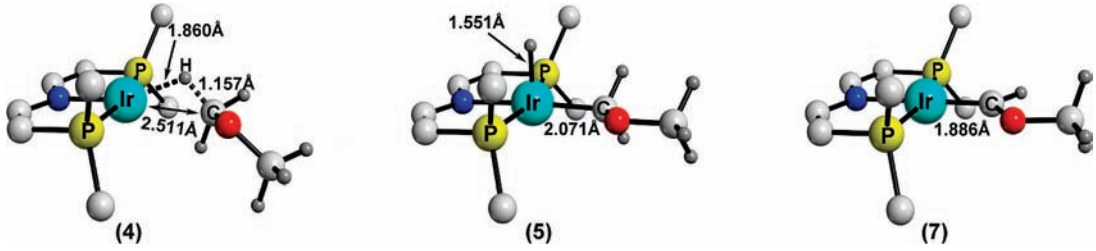

Figure 2. Geometries of selected model compounds, including intermediate structure **4**, highlighting the three-center agostic interaction prior to formation of **5**. Hydrogens are omitted from the [Ir] fragment.

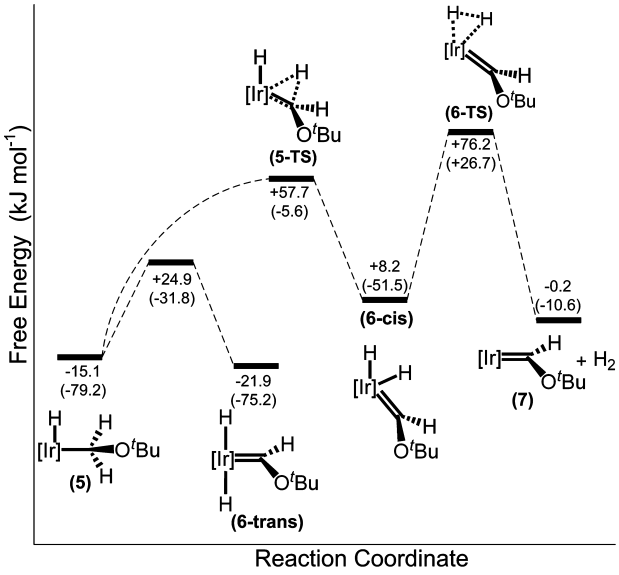

Figure 3. Potential energy surface for the formation of carbene **7**. Values in normal script are Gibbs corrected and those in parentheses are uncorrected electronic energies. All values in kJ mol^{-1}.

equilibrium concentrations. Indeed, the dominant species present would be the lowest energy species in equilibrium, that being **6-trans**. This point is evident in the most recent literature[35] whereby **2** is reacted with CH_3NRR' forming $[Ir](H)_2CHNRR'$, the equivalent of **6-trans** but an aminocarbene. In this amine analogue, the "equilibrium interplay" does not exist, thus preventing further reaction.

The specifics of bond rearrangement throughout this oxidative addition/reductive elimination process can be viewed in diagrams and table form in the Supporting Information. Although this aspect is beyond the scope of the article, it is interesting information and provides an excellent example of the low-energy interplay between the classical and nonclassical forms of dihydrogen bonding of iridium complexes, as well as the trans influence to reductive elimination.

The interplay between the three reactions discussed creates an interesting (autocatalytic-like) cyclic mechanism as illustrated in Scheme 4. First, starting from the left, reaction Figure 1 generates N moles of stable **5** from starting material **1**. Reaction Figure 3 then produces a small quantity of end product **7**, say n_1 moles, along with the same quantity of dihydrogen. The n_1 moles of dihydrogen can then react with stable **5** in Figure 4 to regenerate the starting material and solvent. The overall outcome from this one cycle is a small quantity (n_1 moles) of desired product **7**. The dihydrogen reaction in Figure 4 provides sufficient energy to repeat the cycle until **7** is obtained in quantitative yields and two equivalents of norbornylene is consumed. This proposed slow rate-determining cycle nicely matches that seen experimentally.[13,14]

Oxygen-Atom Transfer from Carbon Dioxide to a Fischer Carbene at (PNP)Ir. Experimentally, carbon dioxide reacts with iridium carbene **7** to form iridium carbonyl [Ir]CO (**15**) and *t*-butyl formate.[13] Low-temperature ^{1}H NMR analysis indicated that a four-membered metallacycle is an intermediate species with a suggested pathway being oxygen-atom metathesis from CO_2 to the metal-bound Fischer alkoxycarbene.[13] Our calculations, as outlined in Figure 6 are in general agreement with this proposal and our analysis highlights some of the intricacies noted within this mechanism.

The initial encounter of the Fischer alkoxycarbene **7** with the linear carbon dioxide is from above the (PNP)Ir plane such that coordination occurs via the filled d_{z^2} metal orbital and the empty π^* of CO_2 (see **7-TS** in Figure 7). The increased electronic density in the π^* orbital distorts the CO_2 into a bent geometry and destabilizes it thermodynamically. This destabilization, as found in much of our recent CO_2 scission analysis,[36] results in transition structure **7-TS** having a free energy +105.8 kJ mol^{-1} above the initial reactants. This barrier is broadly attributed to the breakdown of the π bond in the incoming CO_2 species. Once this barrier is overcome, a stable intermediate **12** is observed such that a four-membered ring between one side of the CO_2 molecule and the iridium carbene has formed.

Some interesting subtleties can be found in this initial four-membered ring formation. First, the donation of electrons into the CO_2 π^* orbital increases the C1−O2 bond length from 1.170 to 1.271 Å in **7-TS** (see Figure 7). Second the metal−carbene Ir−C2 bond is similarly found to increase in length (see Figure

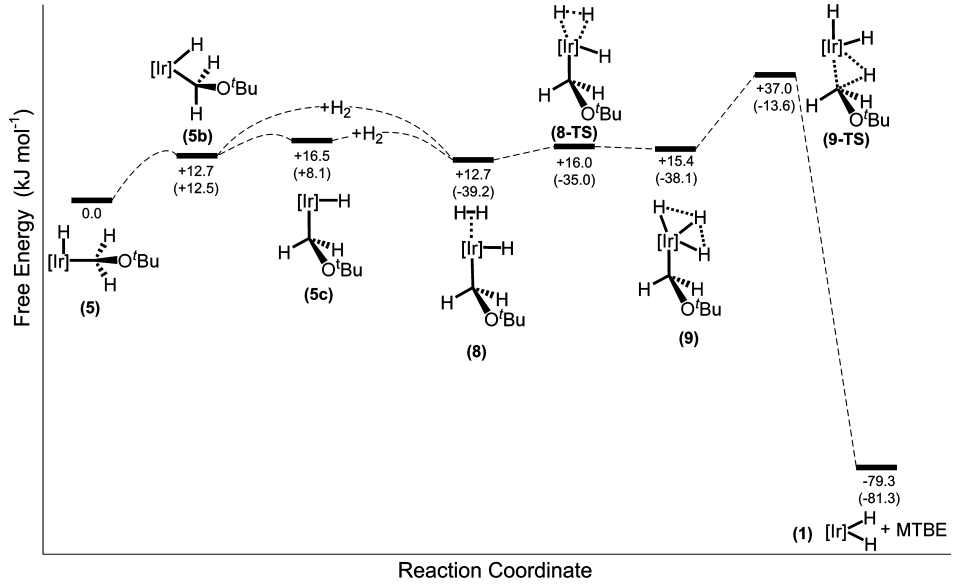

Figure 4. Interaction between the generated H_2 and the MTBE adduct (**5**) to regenerate **1**. Values in normal script are Gibbs corrected, and those in parentheses are uncorrected electronic energies. All values in kJ mol^{-1}.

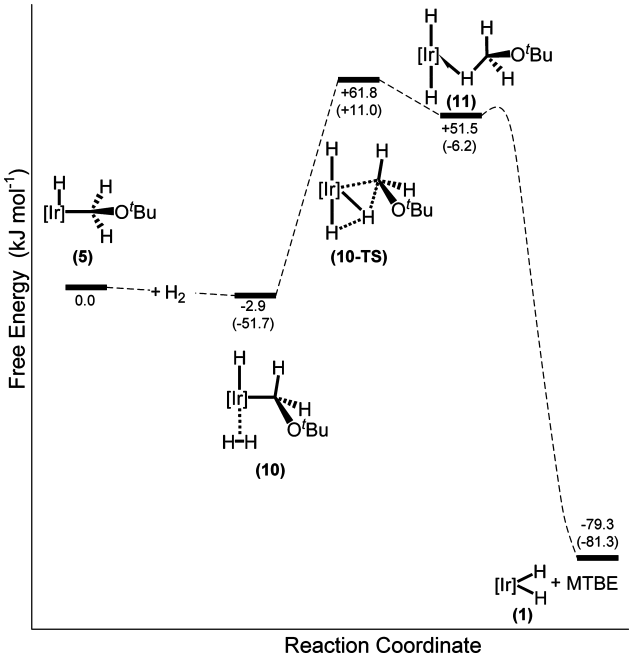

Figure 5. Alternate pathway whereby the H_2 interaction is trans to the bound hydrogen of the ground-state **5** structure. Values in normal script are Gibbs corrected, and those in parentheses are uncorrected electronic energies. All values in kJ mol^{-1}.

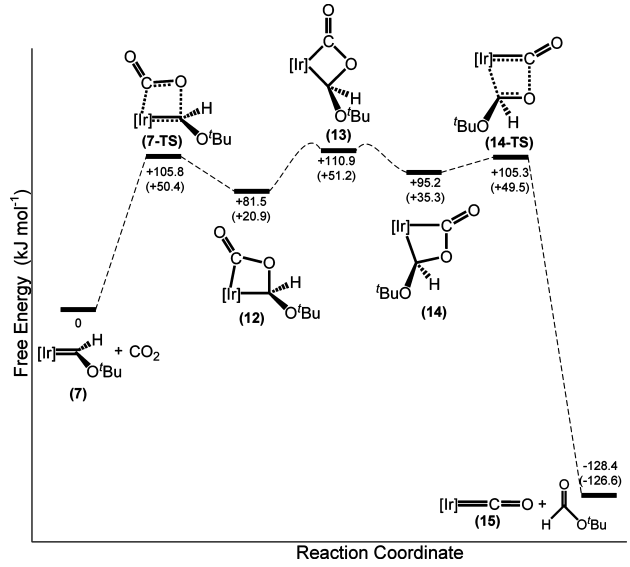

Figure 6. Interaction between CO_2 and an iridium-supported Fischer carbene **7**. Values in normal script are Gibbs corrected, and those in parentheses are uncorrected electronic energies. All values in kJ mol^{-1}.

7) from 1.886 Å in **7** to 1.979 Å in **7-TS**, and finally, but contrary to expectations, the Mulliken electron density on the metal increases from −0.029 in **7** to −0.275 in **7-TS**. These three points at first seem at odds; how is it possible to donate electrons from the metal yet increase its electron density? The contradiction can be overcome by considering the bonding molecular orbitals and the natural bond order electron densities involved in this interaction. Figure 8 provides a simplistic visual representation of the interaction. Initially **7** has the classic σ Fischer carbene donation and metal $d_{yz} \rightarrow \pi$ back-donation. As the carbon dioxide approaches the [Ir] center, a bond is formed by donation of electron density from the filled d_{z^2} orbital of iridium to the π^* orbital of CO_2, which leads to a lengthening of the C1−O2 bond. The proximity of the electron-rich CO_2 oxygen disrupts the Fischer carbene $d_{yz} \rightarrow \pi$ electron back-donation from the metal, lengthening the Ir−C2 bond and returning electron density back to the metal. This is confirmed by NBO analysis, which shows the metal d_{z^2} electron density

Scheme 4

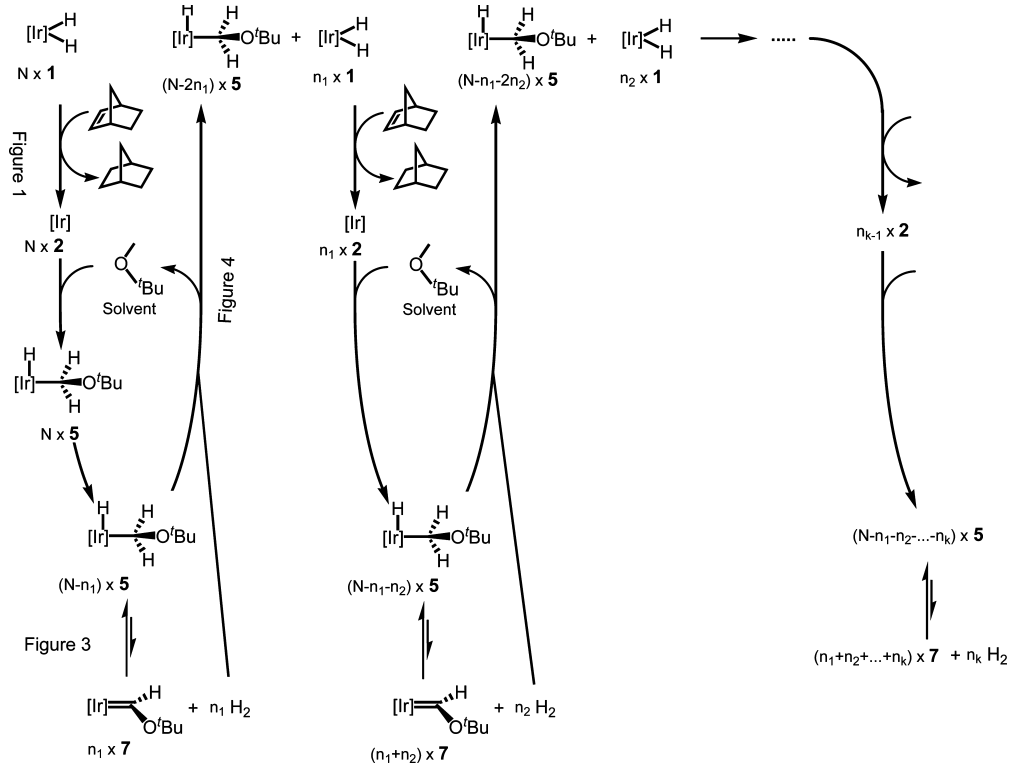

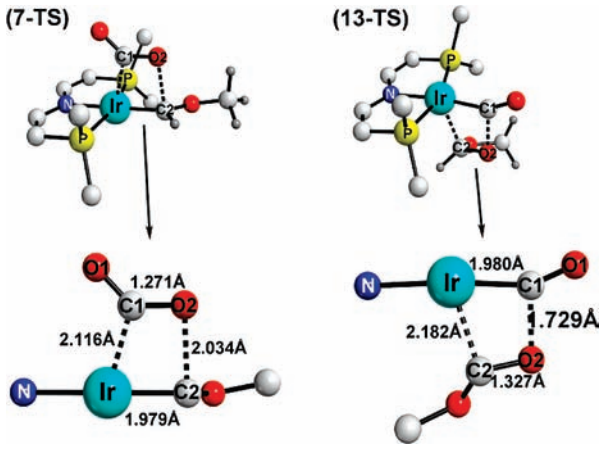

Figure 7. Moldraw diagram of **7-TS** and **13-TS** with the central metallacycle enlarged.

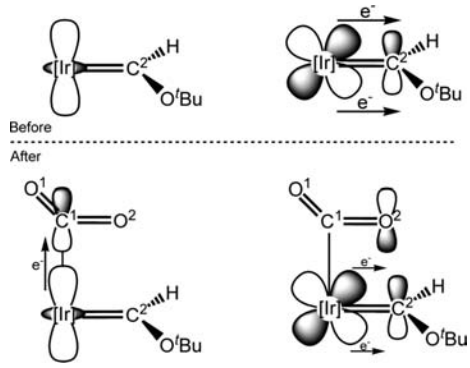

Figure 8. Schematic diagram outlining the electron donation before (above) and after (below) the CO_2 interaction. The left side shows donation from the filled d orbital of iridium to the empty π^* CO_2 orbital, and the right side shows the disruption to the Ir→C2 back-donation caused by the filled π-bonding CO_2 orbital.

reduces from 1.89 to 1.50 but the d_{yz} increases from 1.49 to 1.79. The final formation of **12** involves further rearrangement of bonding orbitals, but the overall concept is that of electron movement around the four membered ring that results in weak Ir−C2 and C1−O2 bonds and formation of Ir−C1 and C2−O2 bonds. Further details of bond lengths and charge distribution can be found in the Supporting Information.

Once the ring has formed, our calculations suggest that structure **12** rearranges to **13** and on to **14** along a very flat potential surface (see Figure 6), whereby scission of the C1−O2 and Ir−C2 can occur at transition structure **14-TS** having a calculated barrier height of +105.3 kJ mol^{-1}. This transition structure has an almost identical but inverted ring arrangement to that found in the initial ring forming transition structure **7-TS**. Clearly the ring breaking mechanism is identical to that of the formation mechanism vide supra, with the exception that the weaker bonds are now Ir−C2 and C1−O2. The overall driving force for the reaction is the stability of the [Ir] carbonyl end product **15**.

Preferential Cleavage of the CS and CN Bonds in OCS and PhNCO. The reaction of Fischer alkoxycarbene **7** with other oxygen-containing heterocumulenes such as carbonyl sulfide and phenyl isocyanide was found[13] to generate the same iridium carbonyl **15** and the corresponding thioformate and formimidate products. Oxygen-atom transfer was not reported in these reactions, no intermediate species were detected during the reactions, and the same four-membered metallacyclic intermediate pathway was predicted. Our calculations are in agreement with the experimental predictions in that a four-membered metallacyclic mechanism is present in almost identical fashion to the CO_2 reaction. However, the selectivity provided by the iridium carbene **7** in the cleavage of CS and CN over CO warrants additional reporting.

First consider the reaction of **7** with SCO. As with the CO_2 interaction, the initial coordination takes place from the d_{z^2} orbital of iridium and the π^* SCO orbital. Due to the asymmetry of SCO, initial coordination can take place with either the sulfur or oxygen proximal to the carbene group. Figure 9 outlines the overall profile, with the central point indicating that the reaction can proceed to either left or right depending on coordination direction.

Clearly the most favorable pathway in Figure 9 is to the right where the maximum barrier is +86.5 kJ mol^{-1} lower and the final product (**15**) is 33.9 kJ mol^{-1} more exothermic. The right-hand pathway is where the sulfur is proximal to the carbene and the four-membered metallacyclic intermediates (**OCS12** and **OCS14**) contain sulfur rather than oxygen. The reason for this clear preference for binding and cleavage of C═S rather than C═O is related to the difference in overall strength of the bonds. The C═S bond in S═C═O is weaker than the C═O, both in terms of its σ[37] and π[28] character, so the kinetic barrier to metallocyclic formation and breakdown will be smaller for the weaker bonds. The overall thermodynamic driving force leads toward the more stable metal carbonyl species **15**, thus also favoring cleavage of C═S.

The interaction with Ph−N═C═O follows a similar trend to that found with carbonyl sulfide. That is, the preferred kinetic pathway involves cleavage of the slightly weaker C═N bond[37,38] rather than the C═O. This is highlighted in Figure 10 where the maximum transition barrier to C═N cleavage to the right is +93.4 kJ mol^{-1} while C═O cleavage to the left is +113.0 kJ mol^{-1}. The kinetic difference in this case is less pronounced, but contrasting this is the thermodynamic difference in the stability of the end products with [Ir]−CO being significantly more stable than [Ir]−NPh.

The kinetic barriers in each of the cases presented can be used to create a simplistic order of bond strengths in the creation/breakdown of the four-membered metallacyclic ring found in this series of reactions. If the transition energies are placed in order, it provides a not-unexpected order of bond strengths, with the C═O and C═S bonds in S═C═O being the strongest and weakest, respectively.

C=O (in S=C=O)	>>	C=O (in N=C=O)	>	C=O (in CO_2)	>	C=N (in N=C=O)	>>	C=S (in S=C=O)
151.6 kJ mol^{-1}		113.0 kJ mol^{-1}		105.8 kJ mol^{-1}		93.4 kJ mol^{-1}		65.1 kJ mol^{-1}

In light of the C═O, C═S, and C═N bond strength discussion some additional comments can be made in regard to both Figures 9 and 10. First, as discussed above, the high-energy transition structure **SCO14-TS** can be explained in terms of the significant energy required to break the strongest C−O σ bond, and so it

(34) Lin, Z. Y.; Hall, M. B. *Coord. Chem. Rev.* **1994**, *135*, 845–879.
(35) Whited, M. T.; Grubbs, R. H. *Organometallics* **2008**, *27*, 5737–5740.
(36) Brookes, N. J.; Ariafard, A.; Stranger, R.; Yates, B. F, 2009, in preparation.
(37) Luo, Y.-R. *Handbook of Bond Dissociation Energies in Organic Compounds*; CRC Press: Boca Raton, FL, 2003.
(38) Galbraith, J. M.; Blank, E.; Shaik, S.; Hiberty, P. C. *Chem.—Eur. J.* **2000**, *6*, 2425–2434.

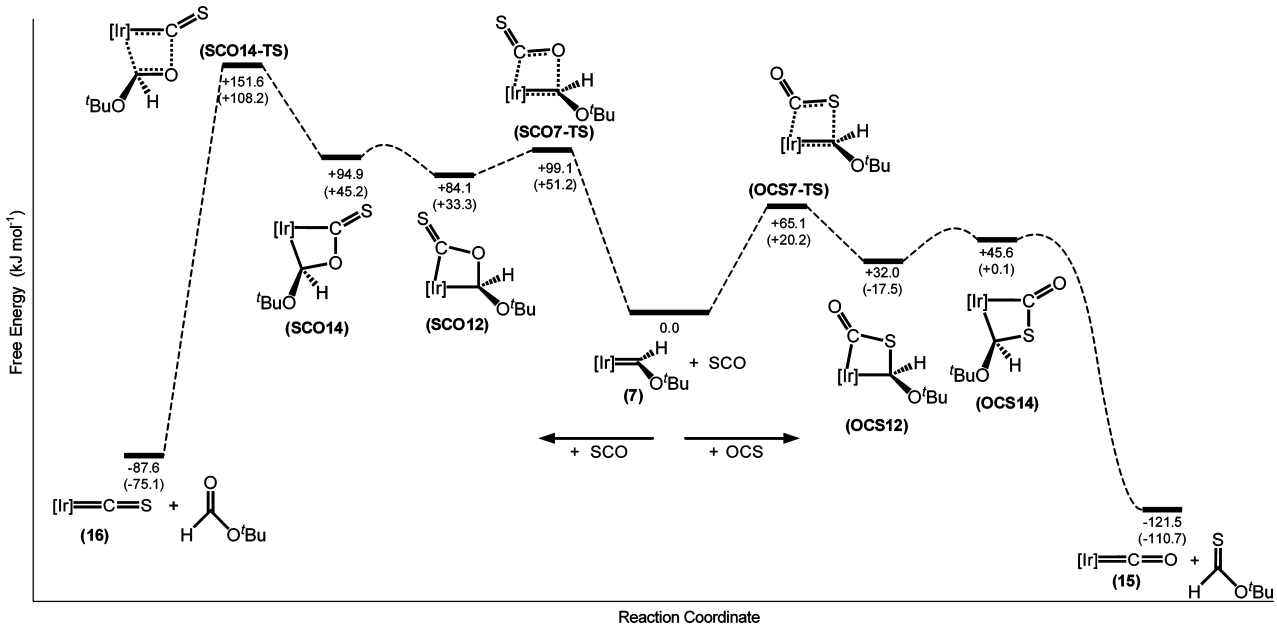

Figure 9. Reaction of **7** with SCO. Left of center is with oxygen proximal to the carbene, and right of center is sulfur proximal to the carbene. Values in normal script are Gibbs corrected, and those in parentheses are uncorrected electronic energies. All values in kJ mol^{-1}.

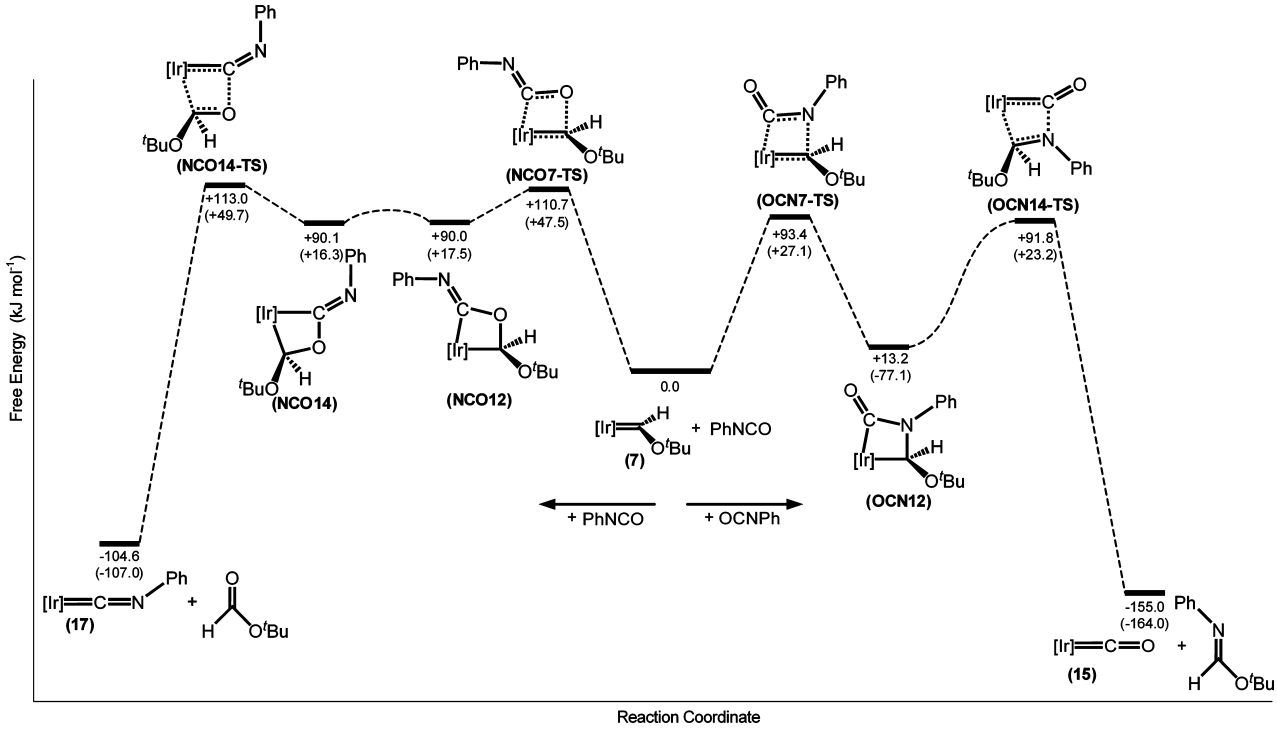

Figure 10. Reaction of **7** with Ph−N=C=O. Left of center is with oxygen proximal to the carbene, and right of center is nitrogen proximal to the carbene. Values in normal script are Gibbs corrected, and those in parentheses are uncorrected electronic energies. All values in kJ mol^{-1}.

is not surprising to find the barrier to breaking the weakest bond in the series, C−S in **OCS14**, is small. In fact our calculations were unable to converge to a stable transition structure **OCS14-TS** due to its closeness in energy to the intermediate **OCS14**; hence, this transition structure point has not been included in Figure 9. Second, the overall stability of **15** compared with its reactants in Figures 9 and 10 has been mentioned above and specifically it provides a thermodynamic driving force to the preferred pathway. But this is somewhat unusual given that the overall reaction appears isodesmic. The stability of the Ir−CO (**15**) is clearly the reason for the low energy and, in bonding terms, the isodesmic nature of the reactants and products is broken by the significant triple bonded character of bound CO groups. The optimized CO bond lengths of 1.167 and 1.186 Å in **15** and PhNCO, respectively, highlight this fact. Finally, but unfortunately not conclusively, structure **OCN12** in Figure 10 is remarkably stable in comparison to all other profiles. The expected intermediate **OCN14** could not be located on the surface since all metallacyclic OCN structures converged to this stable **OCN12**. One might presume the stability of **OCN12**

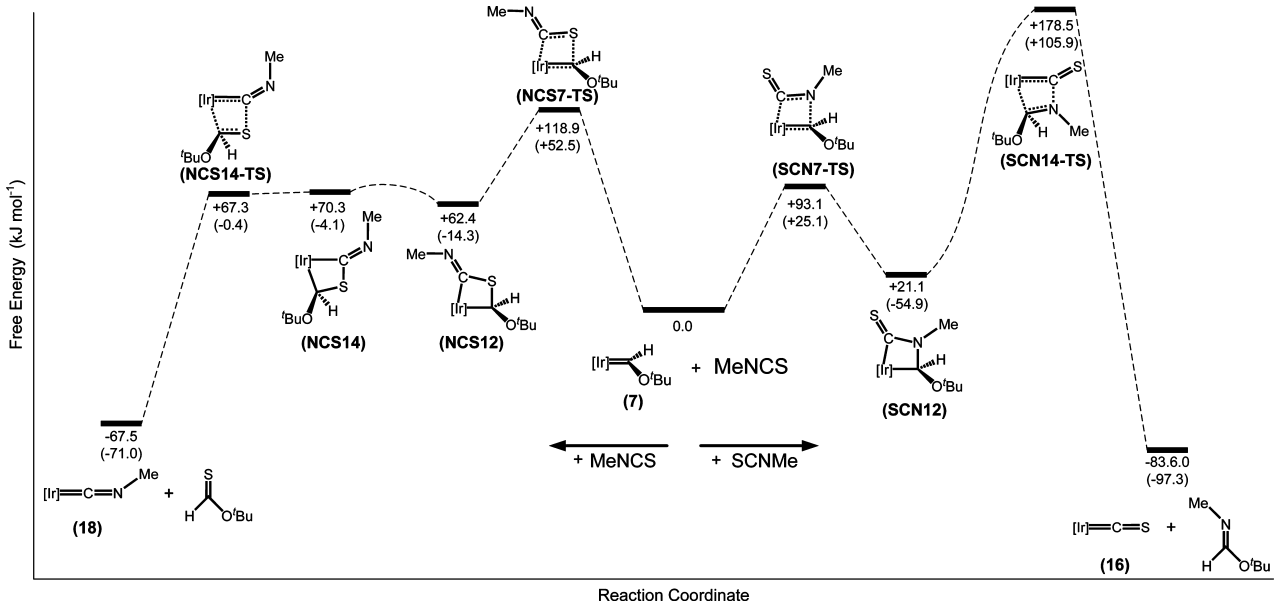

Figure 11. Reaction of **7** with Me−N═C═S. Left of center is with sulfur proximal to the carbene, and right of center is nitrogen proximal to the carbene. Values in normal script are Gibbs corrected, and those in parentheses are uncorrected electronic energies. All values in kJ mol^{-1}.

Scheme 5

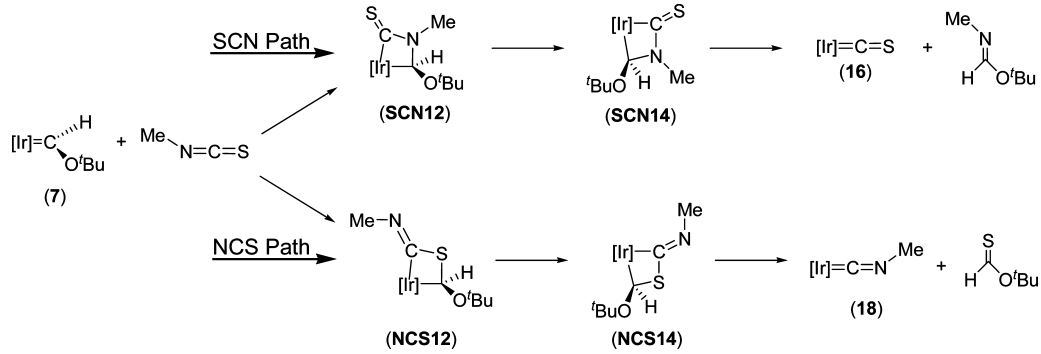

implies a significant difference between π and σ bond strengths in C═N structures, however more work is required to explore this concept.[38−42]

Armed with our table of bond strengths and the fine subtleties derived about Ir−CO stability and π and σ bond strength differences, it may be possible to predict bond cleavage selectivity in other electrophiles which react with **7**. A good example might be SCN$^-$ in say SCN−Me as outlined in Scheme 5.

Here we have a stronger C═N than C═S bond, similar π and σ bond strengths for C═S but different for C═N, and last an Ir═C═S (**16**) product that is more stable than the equivalent Ir═C═N−Me (**18**). From this we might make the following predictions. (1) The weaker C═S bond cleavage pathway (NCS) will have a lower kinetic barrier than the C═N cleavage pathway (SCN), but (2) the more stable [Ir]═C═S product will thermodynamically favor the C═N bond cleavage pathway (SCN). (3) The π and σ differences may cause a very stable encounter complex **SCN12** and a high barrier to breaking the C−N σ bond in **SCN14**. Conversely, we expect a low barrier to breaking the σ C−S bond in **NCS14** and a flat potential energy surface once the first transition structure to**NCS12** is passed.

Overall the predictions lean toward the NCS pathway to cleavage of the C═S bond in MeNCS. These predictions can be confirmed computationally as seen in Figure 11. The lower kinetic pathway of NCS to the left is clearly preferred. It will be interesting to see if this can be verified by experiment.[43]

Conclusion

In this theoretical study we have outlined some important aspects of low-valent iridium chemistry involving PNP ligands. First, we have identified the mechanistic pathway for formation of the alkoxycarbene (PNP)IrC(H)O^{t}Bu. This formation reaction involves a rapid step to a low-energy intermediate which unfortunately can only produce tiny equilibrium concentrations of the sought carbene. The fascinating aspect of this equilibrium is, however, that one of the equilibrium 'byproduct', hydrogen, reacts with the already formed intermediate, pushing the equilibrium toward product formation and providing the necessary thermodynamic driving force necessary for complete conversion to the alkoxycarbene (PNP)IrC(H)O^{t}Bu. This thermodynamic autocatalytic behavior has not been associated with pincer-type iridium PNP chemistry previously and should provide for interesting experimental reaction rate analysis.

(39) Jug, K.; Hiberty, P. C.; Shaik, S. *Chem. Rev.* **2001**, *101*, 1477–1500.
(40) Schmidt, M. W.; Truong, P. N.; Gordon, M. S. *J. Am. Chem. Soc.* **1987**, *109*, 5217–27.
(41) Schleyer, P. V.; Kost, D. *J. Am. Chem. Soc.* **1988**, *110*, 2105–2109.
(42) Wiberg, K. B.; Nakaji, D. *J. Am. Chem. Soc.* **1993**, *115*, 10658–10664.

Second, we found that the addition of CO_2 to the alkoxycarbene to cleave one C═O bond does occur via a four-membered metallacycle between the Fischer carbene and the carbon dioxide. The mechanistic subtleties involve initial interaction between the metal d_{z^2} and empty π^* CO_2 orbitals, four-membered ring formation, rotation of the ring, and finally cleavage of the original iridium carbene and C═O bond of CO_2. This mechanism is in stark contrast to those observed for metal boryls[3,11] and low-coordinate iron complexes.[4] Finally, the reason for preferential cleavage of CS and CN bonds in OCS and PhNCO, respectively, has been revealed. Ultimately the simplistic concept that preferential cleavage occurs for the weaker bond holds true, and mechanistic subtleties within the reaction can be attributed to the strength/weakness of the π and σ bond components. In fact, this approach can be used to make predictions concerning similar reactions between the (PNP)iridium carbene and other small multiply bonded electrophiles.

This study complements the findings found experimentally. It highlights the mechanistic complexity in formation of the iridium carbenes and the subtle but distinct olefin metathesis-like reactivity of the carbenes to small, often inert, electrophiles. This unusual CO_2 activation pathway via increased carbene electrophilicity might point to a more general strategy for activation of strong bonds across M−L multiple bonds. In addition, continued theoretical tuning of the iridium carbene ligand system may uncover other novel substrates that can cleave small multiply bonded molecules and importantly destabilize the end product, thus allowing catalytic activity.[44]

Acknowledgment. We thank the Australian Research Council (ARC) for project funding. We are also indebted to the Australian Partnership for Advanced Computing (APAC) and the Tasmanian Partnership for Advanced Computing (TPAC) for a generous time grant on their parallel computing facilities.

Supporting Information Available: Computational details of all structures (Cartesian coordinates, energies, and solvation calculations) and model chemistries; full refs 5 and 27. This material is available free of charge via the Internet at http://pubs.acs.org.

JA809320X

(43) During manuscript review an article was published which supports preferential CS cleavage, (Ref: Whited, M. T.; Grubbs, R. H. *Organometallics* 2009, *28*, 161−166.)

(44) Whited, M. T.; Grubbs, R. H. *J. Am. Chem. Soc.* **2008**, *130*, 16476–16477.